ISSN 2618-1584 Vol. 7, Issue 6: 1-14, DOI: 10.25236/FMSR.2025.070601

Identification of Ferroptosis-Related Hub Genes and Machine Learning Algorithms in NAFLD-Induced Liver Fibrosis

Siyu Wei[1,a,#], Zhengjie Li[1,b,#], Hongping Mo[1,c], Mingming Song[1,d], Rui Liu[1,e], Tao Pan[1,f,*], Xudong Wen[1,g,*]

[1]Department of Gastroenterology, Chengdu University of Traditional Chinese Medicine Affiliated Hospital of Integrated Traditional Chinese and Western Medicine, Chengdu, China
[a]weisiyu0330@163.com, [b]lizhengjie@stu.cdutcm.edu.cn, [c]mshitangtang@163.com, [d]15983135482@163.com, [e]lr2456429521@163.com, [f]pant414@163.com, [g]xudongwen@cdutcm.edu.cn
**Corresponding author*
[#]These authors contributed equally to this work

Abstract: *Ferroptosis has been recognized as a pivotal mechanism in the progression of liver fibrosis and nonalcoholic fatty liver disease (NAFLD), yet its role in NAFLD-induced liver fibrosis (NILF) remains poorly characterized, and reliable diagnostic biomarkers are currently lacking. To address this gap, we employed an integrated bioinformatics approach to identify ferroptosis-related biomarkers for NILF. Transcriptomic data from patients with NILF were obtained from the Gene Expression Omnibus (GEO) database, and ferroptosis-related genes were collected from FerrDb. Key module genes were screened by weighted gene co-expression network analysis (WGCNA), and their intersection with ferroptosis-related genes was subsequently analyzed via protein-protein interaction (PPI) network to identify candidate hub genes. Three machine learning algorithms—LASSO, random forest, and SVM-RFE—were applied to refine the candidate genes, leading to the identification of four central hub genes (IL1B, IL6, SOCS1, TNFAIP3). These genes demonstrated high diagnostic accuracy for NILF (AUC = 0.974). Furthermore, drug prediction analysis indicated that cycloheximide, profenamine, dexamethasone, and chromium compounds may target these hub genes, suggesting their therapeutic potential. Our study reveals novel ferroptosis-linked biomarkers with diagnostic and therapeutic relevance for NILF, offering insights for early detection and targeted intervention.*

Keywords: *NAFLD-Induced Liver Fibrosis, Ferroptosis, Machine Learning, Biomarker Identification*

1. Introduction

Liver fibrosis induced by viral or metabolic chronic liver diseases poses a significant challenge to global health [1]. Currently, non-alcoholic fatty liver disease-induced liver fibrosis (NILF) is the fastest growing cause of chronic liver disease and may eventually progress to cirrhosis, liver failure and hepatocellular carcinoma, leading to serious consequences [1-3]. Notably, emerging evidence suggests that ferroptosis, an iron-dependent form of regulated cell death characterized by lipid peroxidation, may serve as a critical molecular bridge connecting metabolic dysfunction and fibrotic progression in this context [4]. Thus, it is evident that early identification and diagnosis of NILF, coupled with timely intervention to halt fibrosis progression, are crucial.

In current clinical practice, the diagnosis and monitoring of NILF predominantly rely on invasive procedures such as liver biopsy and conventional serum biomarkers, which are significantly limited by sampling variability, low patient compliance, and late-stage detection capabilities [5-7]. The emerging reliability of bioinformatics approaches in decoding multi-omics networks, as evidenced by a systematic review demonstrating the capacity to resolve steatotic liver diseases heterogeneity through genomics and proteomics integration [8], provides new opportunities for developing non-invasive biomarkers with improved accuracy in fibro-inflammatory staging and therapeutic monitoring. This potential is further substantiated by recent proteomic breakthroughs, exemplified by an aptamer-based screening of 4,738 plasma proteins that identified ADAMTSL2 and an 8-protein panel for non-invasive fibrosis detection in NAFLD [9]. Despite substantial research efforts, current non-invasive approaches continue to face translational challenges. Large-scale clinical validations, exemplified through the

ISSN 2618-1584 Vol. 7, Issue 6: 1-14, DOI: 10.25236/FMSR.2025.070601

LITMUS study's evaluation of 17 biomarkers for advanced NASH fibrosis, have consistently demonstrated suboptimal diagnostic accuracy, with no omics-derived biomarker attaining regulatory approval to date [9-11]. This underscores the urgent need to explore novel biomarkers with high sensitivity and specificity through in-depth molecular network analyses.

The growing recognition of ferroptosis in hepatic pathophysiology provides new research directions. Ferroptosis is intricately linked to the pathogenesis of various liver diseases, including fibrosis, steatohepatitis, and hepatocellular carcinoma [12-14]. In liver fibrosis, the role of ferroptosis mainly has two aspects: first, inhibiting ferroptosis in hepatocytes can reduce iron overload, lipid peroxidation, and inflammatory infiltration during liver injury; second, inducing ferroptosis in hepatic stellate cells can inhibit the formation of liver fibrosis [15]. In NAFLD, iron-induced lipid peroxidation and iron imbalance are closely related to the disease [16]. At present, inducing ferroptosis has emerged as a promising method for treating liver diseases [12, 15, 16]. Evidence confirms that: DHCR7 and 7-DHC represent potential therapeutic targets for ferroptosis-related liver pathologies [17]; BMP4 regulates ferroptosis through GPX4 modulation and constitutes a novel target for NASH therapy [18]; while berberine and exosomal BECN1 induce ferroptosis in hepatic stellate cells to attenuate liver fibrosis [19, 20]. However, despite these mechanistic insights, three critical gaps remain: the role of ferroptosis in liver diseases is still not fully defined, the specific regulatory networks in NILF remain obscure, and we still know very little about the mechanisms and applications of ferroptosis in NILF. Therefore, it is necessary to find a new and accurate method to explore the relationship between NILF and ferroptosis.

In order to better understand the function of genes associated with ferroptosis in NILF and to offer information about the etiology of this disease, this work used a variety of bioinformatics techniques to find possible biomarkers. Using the Gene Expression Omnibus (GEO) database, we looked for possible molecular pathways and used machine learning to identify hub genes and predict possible therapeutic drugs, and we looked at the relationship between ferroptosis-related genes and the development of NILF. In summary, the findings of this study may contribute to the identification and treatment of NILF and expand our understanding of its underlying pathological processes.

2. Materials and methods

2.1 Data Acquisition and Processing

Transcriptome data from three independent cohorts (GSE49541, GSE89632, GSE58979) were obtained from the Gene Expression Omnibus (GEO) database [21], and a ferroptosis-related gene set was retrieved from the FerrDb database [22]. The GSE49541 dataset contained 35 patients with NILF. The GSE89632 dataset included 24 healthy controls (HC) and 18 patients with NILF. GSE58979 dataset included 16 HC and 10 patients with NILF. The expression of all three datasets was obtained from human liver biopsy tissue. On the basis of the Combat function of "ComBat" R package [23], two datasets GSE49541 and GSE89632 were combined, which finally yielded 24 HC and 53 patients with NILF after excluding abnormal samples, were selected as training sets. The dataset GSE58979 was selected as the validation set. The raw data from these GEO datasets were pre-processed and normalized on the basis of the Robust Multiarray Average (RMA) function of "affy" R package [24].

2.2 Differential Expression Genes (DEGs) Analysis

Differential expression genes in the expression series matrix were identified using the "limma" R package [25], with the significance threshold set at an adjusted P-value < 0.05 and $|\log_2 FC| > 1$. The pheatmap" [26] and "ggplot2" [27] R packages were used to visualize the results of DEGs, creating heatmaps and volcano plots.

2.3 Weighted Gene Co-Expression Network Analysis (WGCNA)

Based on the scale-free topology criterion, a co-expression network was constructed using the "WGCNA" R package to identify co-expressed gene modules [28]. Then, we identified genes by the intersection of key module genes and ferroptosis-related genes. Finally, Venn diagram visualization was performed by the online tool Venny 2.1.02 [29].

ISSN 2618-1584 Vol. 7, Issue 6: 1-14, DOI: 10.25236/FMSR.2025.070601

2.4 Functional Enrichment Analysis of Genes

Functional enrichment analysis was performed using the "ClusterProfiler" R package [30] to assess the main biological attributes of degs, specifically gene ontology (GO) and Kyoto Encyclopedia of Genes and Genomes (KEGG) pathway analysis. The threshold was set at P-value < 0.05. GO categories included biological processes (BP), molecular functions (MF) and cellular components (CC) [31].

2.5 Analysis of Protein-Protein Interactions (PPI)

PPI networks were obtained from the Search Tool for the Retrieval Interacting Genes (STRING) database 12.0 (https://cn.string-db.org/) and visualized using Cytoscape 3.9.1 [32]. Candidate hub genes were obtained using CytoHubba and MCODE, plugins provided by Cytoscape.

2.6 Machine Learning Models for Feature Selection and Visualization

Based on the candidate hub genes obtained from the above analysis, the "glmnet" package [33] was used to identify hub genes by least absolute shrinkage and selection operator (LASSO) logistic regression. The specific parameters were: family = "binomial", maxit = 5000, and ten-fold cross validation was used to adjust the optimal value of parameter λ. By this method, a more accurate prediction model can be obtained.

In addition, the "randomforest" R package [34], which determines the optimal number of variables by calculating the average error rate of the candidate hub genes, was used in performing the Random Forest (RF) analysis. A random forest model was built, and the importance score for each candidate hub gene was calculated.

Support Vector Machine (SVM) is capable of handling high-dimensional data, nonlinearly differentiable problems, and is widely used in multiple domains. Using the "msvmrfe" R package [35], SVM-RFE (Recursive Feature Elimination) optimizes the prediction model by reducing the feature vectors generated by the SVM. The final hub genes were identified by intersecting the results from the LASSO, RF, and SVM-RFE analyses.

2.7 Model Evaluation and Comparison

The "tidymodels" R package [36] was used to generate receiver operating characteristic (ROC) curves for the models, and several widely used machine learning algorithms, including Decision Trees (DT), Logistic Regression (LR), Multi-Layer Perceptron (MLP), RF, and SVM-RFE, were used to construct predictive models. The predictive models were evaluated by comparing their accuracy, Brier score, and area under the curve (AUC).

2.8 Drug-Gene Interactions

Drug signatures Database (DsigDB) [37] was used to identify drug molecules that interact with hub genes through the Enrichr platform [38].

3. Results

Detailed procedure of our study is shown in Figure 1.

ISSN 2618-1584 Vol. 7, Issue 6: 1-14, DOI: 10.25236/FMSR.2025.070601

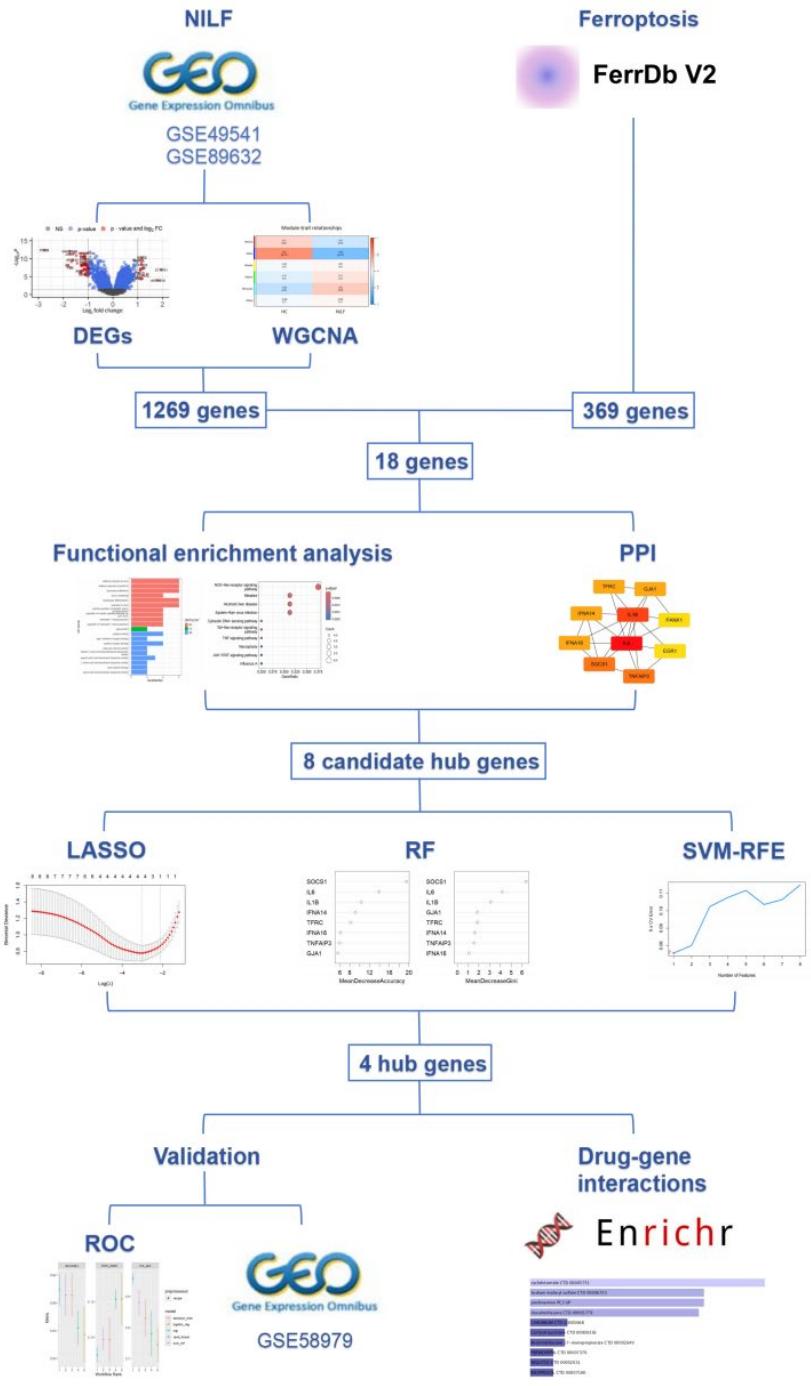

Figure 1: Flow chart.

NILF, NAFLD-induced liver fibrosis; GEO, Gene Expression Omnibus; DEGs, differentially expressed genes; WGCNA, weighted gene co-expression network analysis; PPI, Protein-Protein Interaction; LASSO, the least absolute shrinkage and selection operator; RF, random forest; SVM-RFE, support vector machine - recursive feature elimination; ROC, receiver operating characteristic.

3.1 Identification of DEGs between HC and NILF Patients

To identify potential DEGs, we detected the expression profiles of the GSE49541 and GSE89632 merged data sets from the GEO database using the "limma" package. As a result, a total of 71 DEGs were identified, including 17 up-regulated genes and 54 down-regulated genes. The volcano plot is shown in Figure 2A. The heatmap illustrates the degs between healthy controls and NILF patients (Figure 2B).

ISSN 2618-1584 Vol. 7, Issue 6: 1-14, DOI: 10.25236/FMSR.2025.070601

The combined dataset was used for WGCNA analysis to determine highly correlated gene modules. A scale-free co-expression network was constructed with a soft threshold of 9, showing relatively favorable average connectivity (Figure 2C). We selected 70 as the clustering height threshold to merge highly correlated modules (Figure 2D). Subsequently, 3849 characteristic modules were identified and labeled with different colors (Figure 2E). Finally, we calculated the correlation between each module and clinical characteristics. The results indicated that the MEbrown module was positively correlated with HC (r = 0.21, P = 0.07) and negatively correlated with NILF (r = -0.21, P = 0.07). The MEblue module was positively correlated with HC (r = 0.55, P = 5e-07) and negatively correlated with NILF (r = -0.55, P = 5e-07). The MEturquoise module was negatively correlated with HC (r = -0.28, P = 0.02) and positively correlated with NILF (r = 0.28, P = 0.02) (Figure 2F). Therefore, the MEbrown, MEblue, and MEturquoise modules were identified as clinically significant modules, comprising a total of 1269 genes.

The intersection of 1269 DEGs from clinically significant modules in WGCNA and 246 ferroptosis-related Degs resulted in 18 overlapping ferroptosis-related DEGs in NILF (EGR1, FADS2, GJA1, IL1B, IL6, KDM6B, MAP3K14, NR1D2, PANX1, SLC38A1, SOCS1, TFRC, TNFAIP3, IFNA14, IFNA16, MMD, PEX6, SLC7A11), as illustrated by the Venn diagram (Figure 2G).

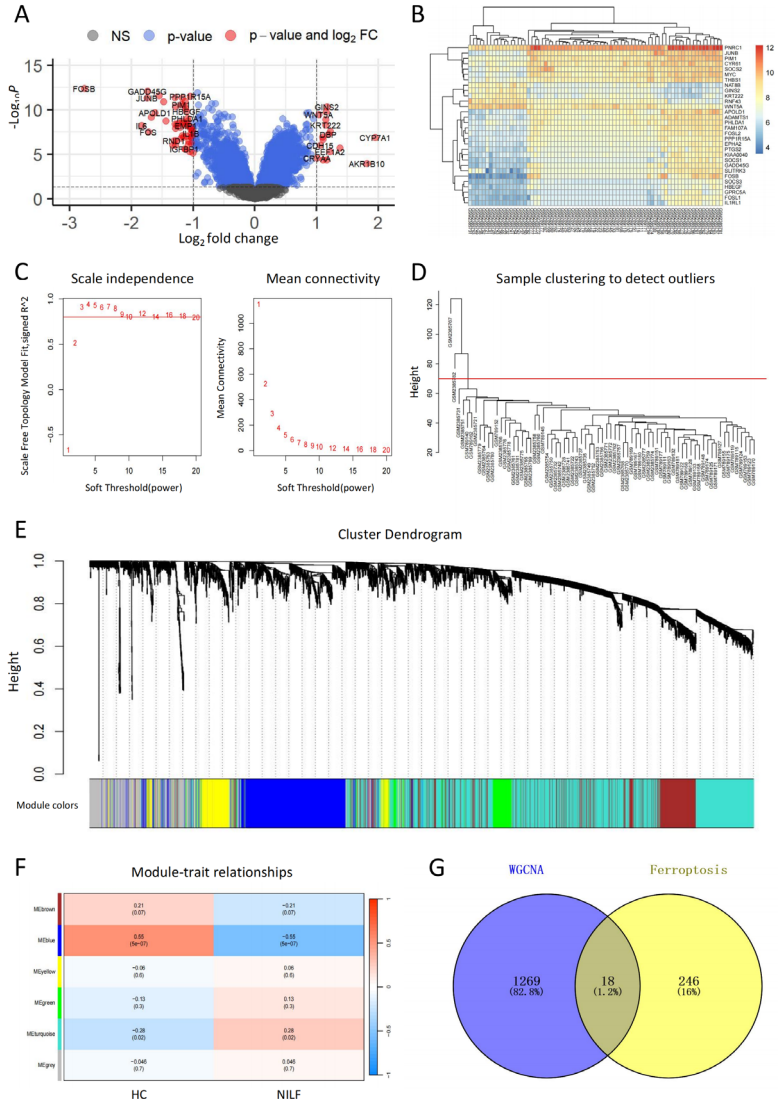

Figure 2: Identification of DEGs and construction of WGCNA co-expression network in NILF. (A) Volcano plot showing DEGs in the NILF and the normal samples. (B) Heat map of DEGs. (C) Soft-thresholding filtering. (D) Sample clustering diagram of WGCNA. (E) Clustering dendrogram of genes. (F) Correlation heatmap of gene modules and clinical features. (G) Venn diagram showing the overlap of DEGs, DEGs in NILF, and ferroptosis-related DEGs.

ISSN 2618-1584 Vol. 7, Issue 6: 1-14, DOI: 10.25236/FMSR.2025.070601

3.2 Functional Enrichment Analysis

Functional enrichment analysis was performed to investigate the biological functions of ferroptosis-related DEGs in NILF in the combined dataset. The GO results indicated that these DEGs were significantly enriched in several BP, including "defense response to virus", "defense response to symbiont", "leukocyte proliferation", "lymphocyte differentiation", and "response to virus"; in the CC "gap junction"; and in MF such as "cytokine activity", "cytokine receptor binding", and "organic anion transmembrane transporter activity" (Figure 3A). Furthermore, KEGG analysis revealed that the DEGs were significantly enriched in the "NOD-like receptor signaling pathway" "measles" and "alcoholic liver disease" (Figure 3B).

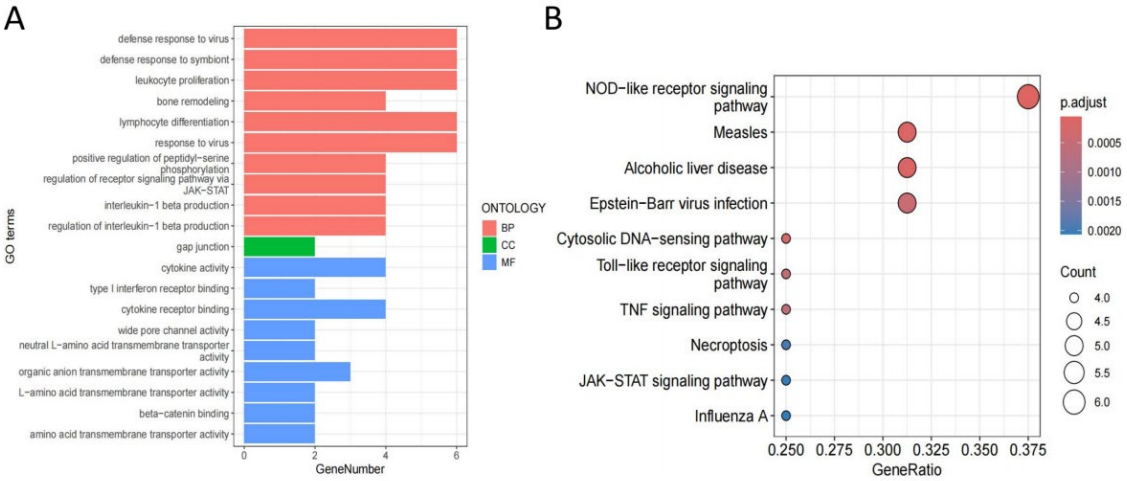

Figure 3: The functional enrichment and generation of ferroptosis-related candidate hub genes. (A) Gene Ontology (GO) enrichment results of 18 Ferroptosis-Related DEGs in NILF. (B) Kyoto Encyclopedia of Genes and Genomes (KEGG) enrichment results of 18 Ferroptosis-Related DEGs in NILF.

3.3 Identification of Ferroptosis-Related Candidate Hub Genes

The STRING database was used to perform PPI analysis on the 18 ferroptosis-related DEGs in NILF (Figure 4A), and network visualization was done using Cytoscape. Using the cytohubba plugin in Cytoscape, the top 10 genes were identified from the PPI network (Figure 4B), among which PANX1 and EGR1 showed significantly lower correlation with the other genes and were therefore manually excluded. Consequently, 8 candidate hub genes were finally identified: "IL6" "IL1B" "TFRC" "GJA1" "IFNA16" "IFNA14" "TNFAIP3" and "SOCS1".

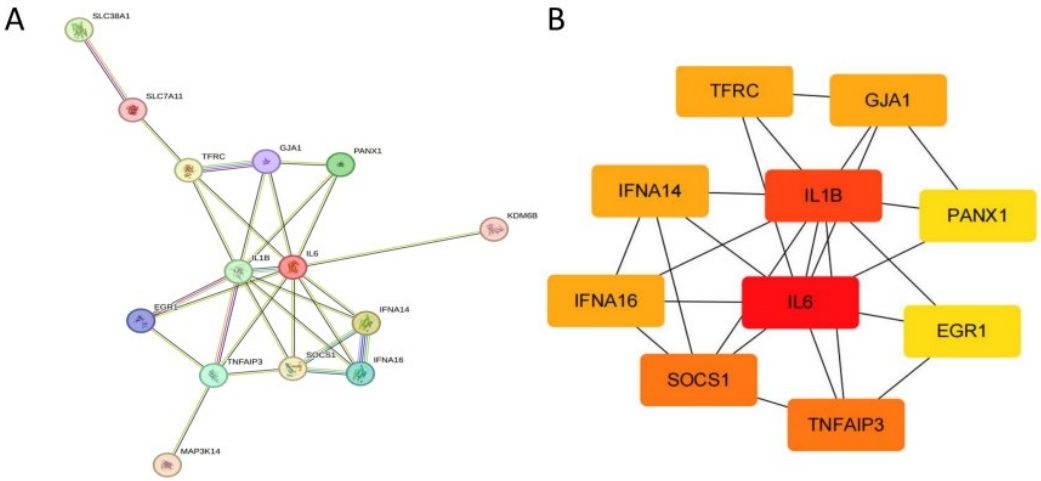

Figure 4: Identification of candidate hub genes. (A) The construction of PPI network. (B) Gene relationship network diagram of 8 candidate hub genes.

ISSN 2618-1584 Vol. 7, Issue 6: 1-14, DOI: 10.25236/FMSR.2025.070601

3.4 Screening of Hub Genes Using Machine Learning Algorithms

The hub genes among the 8 candidate hub genes were identified using LASSO, RF and SVM-RFE. For the LASSO analysis, 4 hub genes (IL1B, IL6, SOCS1, and TNFAIP3) were identified (Figures 5A, B). For the Random Forest analysis, we set the importance value threshold at 0.7 and identified 8 hub genes (Figure 5C). For the SVM-RFE algorithm, 1 hub gene (SOCS1) was selected (Figures 5D, E). Interaction analysis of the three machine learning algorithms indicated that 4 hub genes, IL1B, IL6, SOCS1, and TNFAIP3, were ultimately selected.

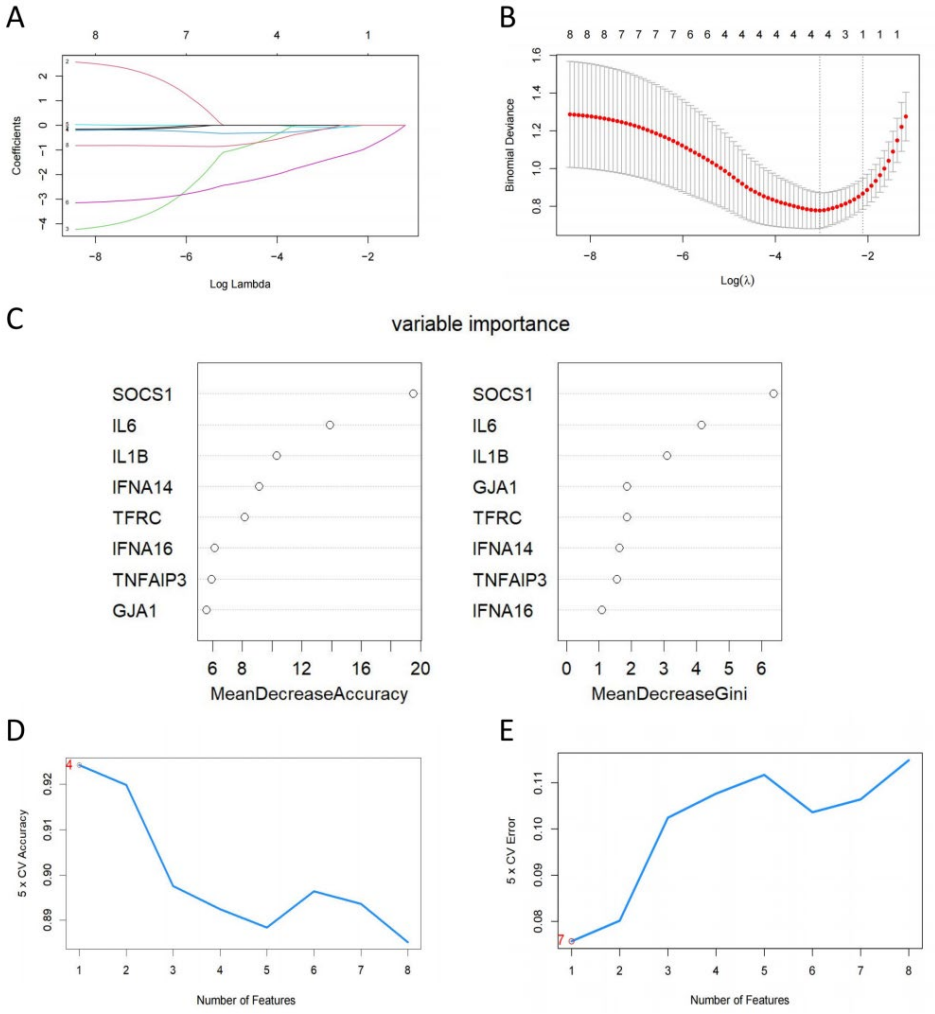

Figure 5: Identification of hub genes for NILF through machine learning. (A) LASSO coefficient profiles of 8 candidate hub genes. (B) Ten-fold cross-validation of LASSO regression analysis. Error bars represented the standard error (SE). The dotted vertical lines corresponded to the optimal value of lambda. (C) Eight genes were overlapped in two ranking methods. (D) The accuracy and (E) the error of the feature selection for the SVM-RFE algorithm. The peak of the curve is achieved at 1 gene with an accuracy of 92.43%, with the lowest cross-validation error is found in 1 gen and the values is 7.57%.

3.5 Validation of Hub Genes

The ROC analysis confirmed that the hub genes identified by the RF algorithm had good predictive performance (Figures 6A, 6B). The AUC under Random Forest was 0.974, indicating that the hub genes have high diagnostic value. The expression levels of the 4 hub genes in HC and NILF samples were presented in box plots, showing that all four hub genes were significantly downregulated in the NILF group (Figures 7A-7D). Additionally, the DEGs in the validation set GSE58979 were identified, showing that all 4 hub genes were significantly downregulated in the validation set (Table 1). In conclusion, we determined that these ferroptosis-related hub genes exhibit good diagnostic capability in predicting the progression of NILF.

ISSN 2618-1584 Vol. 7, Issue 6: 1-14, DOI: 10.25236/FMSR.2025.070601

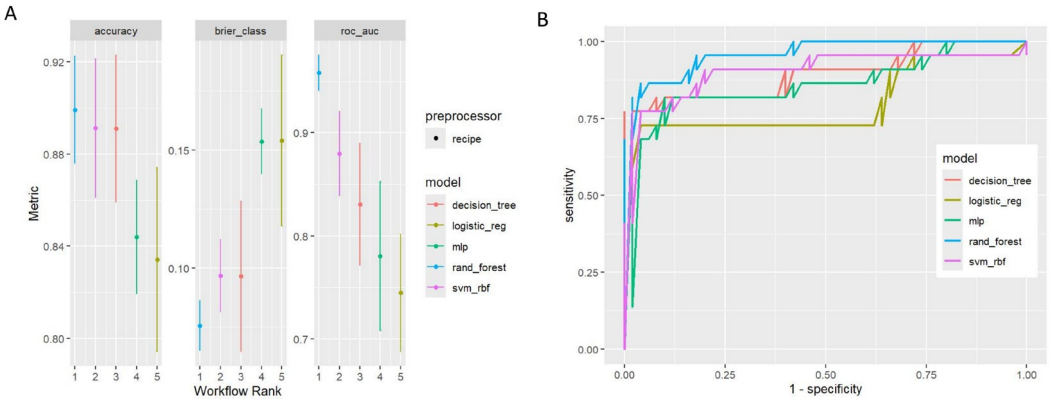

Figure 6: Evaluation of multiple machine learning models by ROC curves. (A) Line plot of multiple machine learning models fitted to three performance. (B) Multi-model ROC curves. The area under the curve (AUC) is used as the evaluation metric.

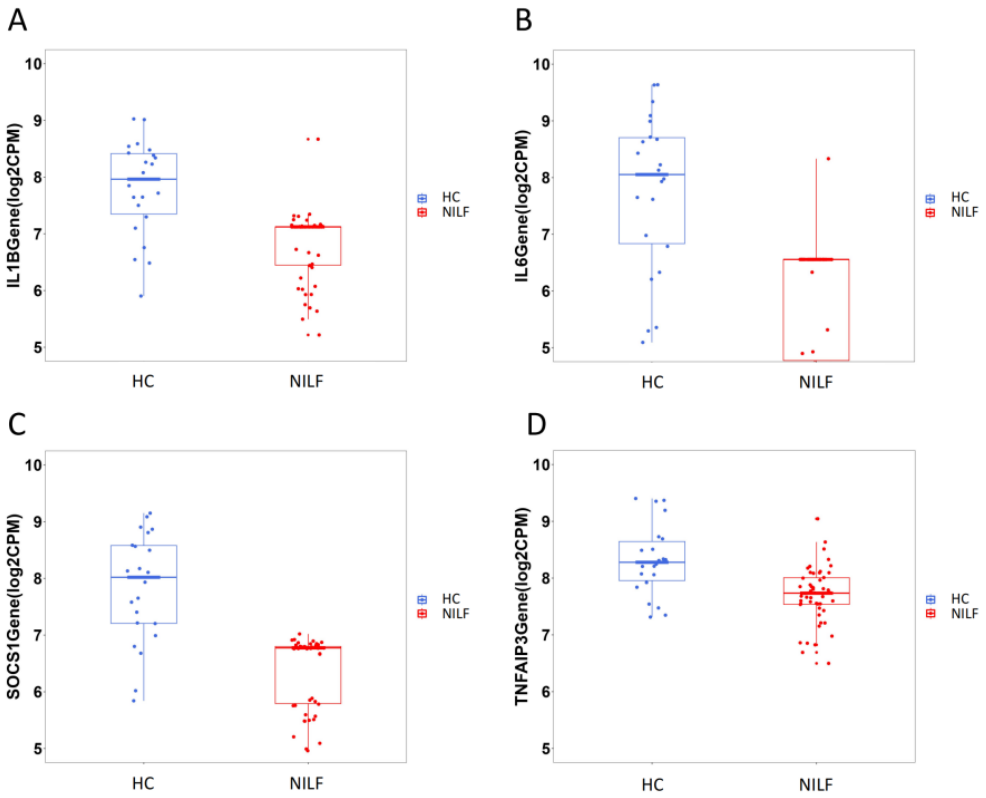

Figure 7: Validation of hub genes. (A-D) Box plots of the expression levels of the three hub genes, including IL1B, IL6, SOCS1 and TNFAIP3.

Table 1 Expression of hub genes in the validation set.

Index	Gene.Symbol	adj.P.Val	P.Value	Log|FC|
1	IL1B	0.03359	0.00264	1.244901
2	IL6	0.027451	0.00182	3.10662409
3	SOCS1	0.060773	0.00742	0.6077356
4	TNFAIP3	0.009679	0.000251	1.417459

3.6 Prediction of Therapeutic Targets

Utilizing bar charts generated from the EnRichr platform based on DSigDB, the interactions between drugs and hub genes were studied. The results indicated that cycloheximide, profenamine, dexamethasone, and CHROMIUM had the highest correlations, suggesting they are the most likely potential therapeutic drugs for NILF (Figure 8A, Table 2).

ISSN 2618-1584 Vol. 7, Issue 6: 1-14, DOI: 10.25236/FMSR.2025.070601

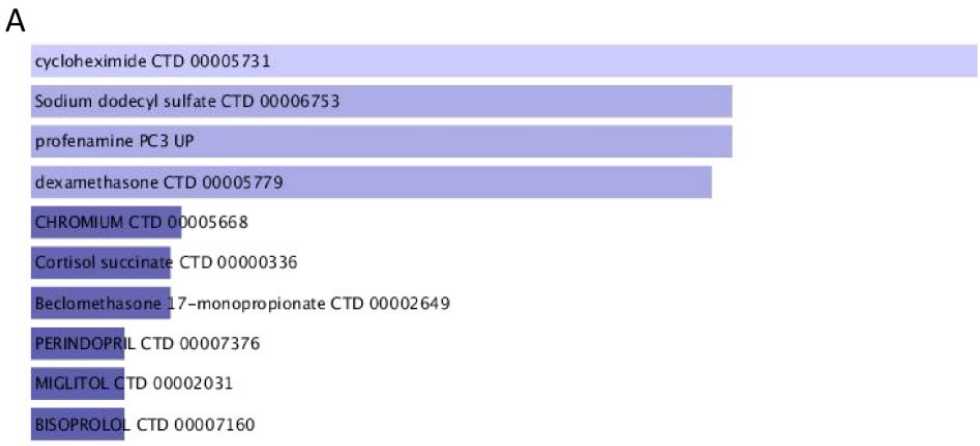

Figure 8: Drug prediction. (A) The bar chart generated on the Enrichr platform based on Drug Signature Database is used to study the interaction between drugs and DEGs.

Table 2 Drug candidates combined with hub genes.

Index	Name	P-value	Adjusted p-value	Odds Ratio	Combined score	Genes
1	cycloheximide CTD 00005731	6.76E-08	6.71E-05	78704	1299355.161	IL6; SOCS1; IL1B; TNFAIP3
2	Sodium dodecyl sulfate CTD 00006753	1.78E-07	6.71E-05	866.3913043	13462.75359	IL6; IL1B; TNFAIP3
3	profenamine PC3 UP	1.78E-07	6.71E-05	866.3913043	13462.75359	IL6; IL1B; TNFAIP3
4	dexamethasone CTD 00005779	1.94E-07	6.71E-05	78316	1210571.467	IL6; SOCS1; IL1B; TNFAIP3
5	CHROMIUM CTD 00005668	1.58E-06	2.27E-04	410.7103448	5486.394159	IL6; IL1B; TNFAIP3
6	Cortisol succinate CTD 00000336	1.65E-06	2.27E-04	2220.777778	29570.47781	IL6; IL1B
7	Beclomethasone 17-monopropionate CTD 00002649	1.65E-06	2.27E-04	2220.777778	29570.47781	IL6; IL1B
8	PERINDOPRIL CTD 00007376	1.98E-06	2.27E-04	1998.6	26247.83934	IL6; IL1B
9	MIGLITOL CTD 00002031	1.98E-06	2.27E-04	1998.6	26247.83934	IL6; IL1B
10	BISOPROLOL CTD 00007160	1.98E-06	2.27E-04	1998.6	26247.83934	IL6; IL1B

ISSN 2618-1584 Vol. 7, Issue 6: 1-14, DOI: 10.25236/FMSR.2025.070601

4. Discussion

This study systematically identified ferroptosis-related hub genes (IL1B, IL6, SOCS1, and TNFAIP3) in NILF through integrated bioinformatics and machine learning approaches, and assessed their clinical relevance as diagnostic biomarkers and therapeutic targets. Furthermore, we identified the key biological pathways significantly enriched by these hub genes through the GO and KEGG pathway analyses, and predicted potential therapeutic compounds. These findings provide mechanistic insights into NILF pathogenesis and lay a theoretical foundation for developing precision diagnostic and therapeutic strategies. However, several critical issues require clarification to strengthen the scientific rigor and translational relevance.

We identified hub genes (IL1B, IL6, SOCS1, and TNFAIP3) with potential diagnostic and therapeutic value for NILF. The functional network formed by these genes underlines the fundamental regulatory mechanisms of inflammation and metabolic dysregulation in NILF. Specifically, as canonical pro-inflammatory cytokines, IL1B and IL6 promote HSC activation and collagen deposition via NF-κB and JAK-STAT pathways, directly stimulating fibrogenesis [39]. In contrast, SOCS1(a suppressor of cytokine signaling)negatively modulates IL6-induced STAT3 phosphorylation to inhibit excessive HSC activation [40], while TNFAIP3 (A20 protein) terminates NOD-like receptor signaling via deubiquitination [41]. The disruption of this pro-inflammatory/anti-inflammatory balance may underpin chronic inflammatory microenvironment in NILF.

Building on these findings, the GO and KEGG pathway analyses revealed critical pathways associated with these hub genes, including "defense response to viruses", "NOD-like receptor signaling pathway", and "gap junction regulation". Of particular interest, the enrichment of the NOD-like receptor signaling pathway (involving all four genes) underscores the central role of pattern recognition receptors (e.g., the NLRP3 inflammasome) in NILF. IL1B, as a downstream effector of NLRP3, requires this pathway for maturation and release, whereas TNFAIP3 may form a protective feedback loop by inhibiting NLRP3 inflammasome assembly [42]. The association with bone remodeling regulation (all four genes involved) likely reflects pathological crosstalk between extracellular matrix (ECM) metabolism and Wnt/β-catenin signaling during HSC transdifferentiation into myofibroblasts [43]. The absence of IL1B (which encodes IL-1β) in the pathway term "regulation of IL-1β production" warrants mechanistic interpretation: (1) IL1B may function primarily as a terminal effector whose transcription is controlled by upstream regulators like NF-κB, rather than being part of its own regulatory pathway; (2) SOCS1 indirectly modulates the synthesis of the IL1B precursor (pro-IL-1β) via TLR4/myd88 suppression rather than directly participating in the generation of mature IL-1β [44, 45].

Importantly, the interplay between the identified hub genes and ferroptosis may drive NILF progression through multidimensional mechanisms. The NLRP3 inflammasome, a core member of the NOD-like receptor family, releases IL1B and IL18 upon activation, directly triggering hepatocyte ferroptosis. Recent studies have revealed that ribosome quality control factor PELO promotes NLRP3 inflammasome-dependent inflammation by activating NLR protein ATPase activity and oligomerization [46]. This aligns with the high IL1B expression in our study, suggesting the NLRP3-PELO axis as a hub for ferroptosis-inflammation crosstalk. Ferroptosis exhibits opposing roles in hepatocytes and hepatic stellate cells (HSCs): hepatocyte ferroptosis activates HSCs via the release of damage-associated molecular patterns (DAMPs), while HSC ferroptosis inhibits fibrosis. Single-cell data have indicated IL6 and IL1B expression across hepatocytes, Kupffer cells, and HSCs, potentially coordinating intercellular crosstalk through paracrine signaling [47, 48]. IL6 may upregulate ACSL4 (a ferroptosis promoter) and suppress GPX4 (a ferroptosis inhibitor) in HSCs via STAT3 activation, modulating their ferroptosis threshold [49, 50]. Gut dysbiosis-derived metabolites (e.g., LPS, indole derivatives) activate NLRP3 inflammasome via TLR4/MyD88 signaling and inhibit SLC7A11-mediated cystine uptake, leading to glutathione depletion and ferroptosis susceptibility [48]. The enrichment of "defense response to viruses" pathways in our study suggests that PAMPs may exacerbate the ferroptosis-fibrosis vicious cycle in NILF through similar mechanisms. Recent animal studies have confirmed that probiotic interventions restore gut microbiota diversity and upregulate FTH1/FTL expression, thereby inhibiting hepatocyte ferroptosis [48, 51]. SOCS1, a JAK-STAT suppressor, may regulate glutathione synthase expression through the mtorc1-ATF4 axis, impacting cellular antioxidant capacity [49, 50]. Additionally, NF-κB binding sites in promoters of ferroptosis-related genes (e.g., GPX4, ACSL4) imply that IL1B/TNFAIP3-mediated inflammatory signals directly modulate ferroptosis-associated epigenetic modifications [46].

Based on the above mechanisms, we identified potential therapeutic drugs associated with these hub genes, including cycloheximide, Sodium dodecyl sulfate, profenamine, dexamethasone, and

ISSN 2618-1584 Vol. 7, Issue 6: 1-14, DOI: 10.25236/FMSR.2025.070601

CHROMIUM. These drugs show a high correlation with key genes related to ferroptosis and may have potential therapeutic effects for NILF. However, further clinical validation and drug development research are needed for these potential therapeutic drugs. Cycloheximide suppresses Erastin-induced ferroptosis by inhibiting ribosome-dependent synthesis of pro-inflammatory mediators (e.g., IL-6/TNF-α), thereby attenuating NILF progression [52]. Profenamine mitigates hepatic fibrogenesis through histamine receptor H1 (HRH1) blockade, reducing TGF-β1-driven activation of hepatic stellate cells [53]. Dexamethasone, a potent glucocorticoid, exerts anti-inflammatory and immunosuppressive effects. Mechanistically, dexamethasone enhances ferroptosis sensitivity by upregulating dipeptidyl peptidase-1 (DPEP1), a regulator of glutathione (GSH) metabolism [54]. Furthermore, numerous studies have advanced the understanding and application of dexamethasone [55, 56]. Future research could explore novel delivery systems or combination therapies incorporating dexamethasone to enhance its efficacy in NILF. Chromium exhibits dichotomous effects: hexavalent chromium (Cr-VI) exacerbates fibrosis via oxidative stress amplification, whereas trivalent chromium (Cr-III) may ameliorate insulin resistance, a key factor in NAFLD/NASH progression; further mechanistic clarification is critical.

This study has limitations requiring consideration. The modest sample size limits statistical power and generalizability, while the bioinformatics-driven design necessitates validation through clinical cohorts and experimental models. Future work should employ multi-center cohorts to enhance sample diversity, integrate multi-omics validation (e.g., transcriptomics/proteomics of patient biopsies), and conduct functional experiments targeting identified hub genes. Such approaches would verify ferroptosis pathomechanisms in NILF and accelerate clinical translation.

5. Conclusions

In summary, the study shows that ferroptosis-related hub genes (IL1B, IL6, SOCS1, TNFAIP3) are identified as dual diagnostic/therapeutic biomarkers for NILF by integrated genomics, bioinformatics, and machine learning approaches, whereas related drug candidates are revealed. These results broaden the knowledge of NILF pathogenesis and provide a basis for individualized therapy, offering crucial theoretical and clinical advice for early diagnosis and prevention. Significant translational potential for future clinical applications is demonstrated by the identified targets and chemicals.

Acknowledgements

We acknowledge Geo (https://www.ncbi.nlm.nih.gov/geo/) database for open access to the database. This study was supported by National Natural Science Foundation of China [grant number 82474299].

Data availability statement

All data for the GSE49541, GSE89632 and GSE58979 datasets can be found in the GEO database (https://www.ncbi.nlm.nih.gov/geo/).

Author contributions

SW, ZL, and HM were responsible for data curation, formal analysis. SW and ZL contributed to methodology, resources, and visualization. MS, and RL were responsible for software screening and application. RL, and TP performed validation. SW, ZL, HM, RL, and MS contributed to writing - original draft. TP participated in conceptualization, investigation, project administration, and supervision. XW led conceptualization, funding acquisition, project administration, supervision, and writing – review & editing.

Conflict of interest

The authors declare that the study was conducted in the absence of any commercial or financial relationship that could be perceived as a potential conflict of interest.

ISSN 2618-1584 Vol. 7, Issue 6: 1-14, DOI: 10.25236/FMSR.2025.070601

References

[1] N. Roehlen, E. Crouchet, T.F. Baumert, Liver Fibrosis: Mechanistic Concepts and Therapeutic Perspectives, Cells, 9(4) (2020).
[2] Z.M. Younossi, A.B. Koenig, D. Abdelatif, Y. Fazel, L. Henry, M. Wymer, Global epidemiology of nonalcoholic fatty liver disease-Meta-analytic assessment of prevalence, incidence, and outcomes, Hepatology, 64(1) (2016) 73-84.
[3] R. Kumar, R.N. Priyadarshi, U. Anand, Non-alcoholic Fatty Liver Disease: Growing Burden, Adverse Outcomes and Associations, J Clin Transl Hepatol, 8(1) (2020) 76-86.
[4] Y. Gong, Z. Liu, Y. Zhang, J. Zhang, Y. Zheng, Z. Wu, AGER1 deficiency-triggered ferroptosis drives fibrosis progression in nonalcoholic steatohepatitis with type 2 diabetes mellitus, Cell Death Discov, 9(1) (2023) 178.
[5] S. Petta, V.W. Wong, C. Cammà, J.B. Hiriart, G.L. Wong, F. Marra, J. Vergniol, A.W. Chan, V. Di Marco, W. Merrouche, H.L. Chan, M. Barbara, B. Le-Bail, U. Arena, A. Craxì, V. de Ledinghen, Improved noninvasive prediction of liver fibrosis by liver stiffness measurement in patients with nonalcoholic fatty liver disease accounting for controlled attenuation parameter values, Hepatology, 65(4) (2017) 1145-1155.
[6] N. Peleg, A. Issachar, O. Sneh-Arbib, A. Shlomai, AST to Platelet Ratio Index and fibrosis 4 calculator scores for non-invasive assessment of hepatic fibrosis in patients with non-alcoholic fatty liver disease, Dig Liver Dis, 49(10) (2017) 1133-1138.
[7] N. Stefan, H.U. Häring, K. Cusi, Non-alcoholic fatty liver disease: causes, diagnosis, cardiometabolic consequences, and treatment strategies, Lancet Diabetes Endocrinol, 7(4) (2019) 313-324.
[8] M. Thiele, I.F. Villesen, L. Niu, S. Johansen, K. Sulek, S. Nishijima, L.V. Espen, M. Keller, M. Israelsen, T. Suvitaival, A. Zawadzki, H.B. Juel, M.J. Brol, S.E. Stinson, Y. Huang, M.C.A. Silva, M. Kuhn, E. Anastasiadou, D.J. Leeming, M. Karsdal, J. Matthijnssens, M. Arumugam, L.T. Dalgaard, C. Legido-Quigley, M. Mann, J. Trebicka, P. Bork, L.J. Jensen, T. Hansen, A. Krag, Opportunities and barriers in omics-based biomarker discovery for steatotic liver diseases, J Hepatol, 81(2) (2024) 345-359.
[9] K.E. Corey, R. Pitts, M. Lai, J. Loureiro, R. Masia, S.A. Osganian, J.L. Gustafson, M.M. Hutter, D.W. Gee, O.R. Meireles, E.R. Witkowski, S.M. Richards, J. Jacob, N. Finkel, D. Ngo, T.J. Wang, R.E. Gerszten, C. Ukomadu, L.L. Jennings, ADAMTSL2 protein and a soluble biomarker signature identify at-risk non-alcoholic steatohepatitis and fibrosis in adults with NAFLD, J Hepatol, 76(1) (2022) 25-33.
[10] Y. Vali, J. Lee, J. Boursier, S. Petta, K. Wonders, D. Tiniakos, P. Bedossa, A. Geier, S. Francque, M. Allison, G. Papatheodoridis, H. Cortez-Pinto, R. Pais, J.F. Dufour, D.J. Leeming, S.A. Harrison, Y. Chen, J.F. Cobbold, M. Pavlides, A.G. Holleboom, H. Yki-Jarvinen, J. Crespo, M. Karsdal, R. Ostroff, M.H. Zafarmand, R. Torstenson, K. Duffin, C. Yunis, C. Brass, M. Ekstedt, G.P. Aithal, J.M. Schattenberg, E. Bugianesi, M. Romero-Gomez, V. Ratziu, Q.M. Anstee, P.M. Bossuyt, Biomarkers for staging fibrosis and non-alcoholic steatohepatitis in non-alcoholic fatty liver disease (the LITMUS project): a comparative diagnostic accuracy study, Lancet Gastroenterol Hepatol, 8(8) (2023) 714-725.
[11] K. Shirabe, Y. Bekki, D. Gantumur, K. Araki, N. Ishii, A. Kuno, H. Narimatsu, M. Mizokami, Mac-2 binding protein glycan isomer (M2BPGi) is a new serum biomarker for assessing liver fibrosis: more than a biomarker of liver fibrosis, J Gastroenterol, 53(7) (2018) 819-826.
[12] Y. Bi, S. Liu, X. Qin, M. Abudureyimu, L. Wang, R. Zou, A. Ajoolabady, W. Zhang, H. Peng, J. Ren, Y. Zhang, FUNDC1 interacts with GPx4 to govern hepatic ferroptosis and fibrotic injury through a mitophagy-dependent manner, J Adv Res, 55 (2024) 45-60.
[13] Z. Zhang, M. Guo, Y. Li, M. Shen, D. Kong, J. Shao, H. Ding, S. Tan, A. Chen, F. Zhang, S. Zheng, RNA-binding protein ZFP36/TTP protects against ferroptosis by regulating autophagy signaling pathway in hepatic stellate cells, Autophagy, 16(8) (2020) 1482-1505.
[14] Z. Zhang, M. Guo, M. Shen, D. Kong, F. Zhang, J. Shao, S. Tan, S. Wang, A. Chen, P. Cao, S. Zheng, The BRD7-P53-SLC25A28 axis regulates ferroptosis in hepatic stellate cells, Redox Biol, 36 (2020) 101619.
[15] J.L. Lu, C.X. Yu, L.J. Song, Programmed cell death in hepatic fibrosis: current and perspectives, Cell Death Discov, 9(1) (2023) 449.
[16] S. Xu, Y. Chen, J. Miao, Y. Li, J. Liu, J. Zhang, J. Liang, S. Chen, S. Hou, Esculin inhibits hepatic stellate cell activation and CCl(4)-induced liver fibrosis by activating the Nrf2/GPX4 signaling pathway, Phytomedicine, 128 (2024) 155465.
[17] N. Yamada, T. Karasawa, J. Ito, D. Yamamuro, K. Morimoto, T. Nakamura, T. Komada, C. Baatarjav, Y. Saimoto, Y. Jinnouchi, K. Watanabe, K. Miura, N. Yahagi, K. Nakagawa, T. Matsumura,

ISSN 2618-1584 Vol. 7, Issue 6: 1-14, DOI: 10.25236/FMSR.2025.070601

K.I. Yamada, S. Ishibashi, N. Sata, M. Conrad, M. Takahashi, Inhibition of 7-dehydrocholesterol reductase prevents hepatic ferroptosis under an active state of sterol synthesis, Nat Commun, 15(1) (2024) 2195.

[18] X. Wang, B. Ma, X. Wen, H. You, C. Sheng, L. Bu, S. Qu, Bone morphogenetic protein 4 alleviates nonalcoholic steatohepatitis by inhibiting hepatic ferroptosis, Cell Death Discov, 8(1) (2022) 234.

[19] Y. Tan, Y. Huang, R. Mei, F. Mao, D. Yang, J. Liu, W. Xu, H. Qian, Y. Yan, HucMSC-derived exosomes delivered BECN1 induces ferroptosis of hepatic stellate cells via regulating the xCT/GPX4 axis, Cell Death Dis, 13(4) (2022) 319.

[20] J. Yi, S. Wu, S. Tan, Y. Qin, X. Wang, J. Jiang, H. Liu, B. Wu, Berberine alleviates liver fibrosis through inducing ferrous redox to activate ROS-mediated hepatic stellate cells ferroptosis, Cell Death Discov, 7(1) (2021) 374.

[21] T. Barrett, D.B. Troup, S.E. Wilhite, P. Ledoux, D. Rudnev, C. Evangelista, I.F. Kim, A. Soboleva, M. Tomashevsky, R. Edgar, NCBI GEO: mining tens of millions of expression profiles--database and tools update, Nucleic Acids Res, 35(Database issue) (2007) D760-5.

[22] N. Zhou, X. Yuan, Q. Du, Z. Zhang, X. Shi, J. Bao, Y. Ning, L. Peng, FerrDb V2: update of the manually curated database of ferroptosis regulators and ferroptosis-disease associations, Nucleic Acids Res, 51(D1) (2023) D571-d582.

[23] W.E. Johnson, C. Li, A. Rabinovic, Adjusting batch effects in microarray expression data using empirical Bayes methods, Biostatistics, 8(1) (2007) 118-27.

[24] L. Gautier, L. Cope, B.M. Bolstad, R.A. Irizarry, affy--analysis of Affymetrix GeneChip data at the probe level, Bioinformatics, 20(3) (2004) 307-15.

[25] M.E. Ritchie, B. Phipson, D. Wu, Y. Hu, C.W. Law, W. Shi, G.K. Smyth, limma powers differential expression analyses for RNA-sequencing and microarray studies, Nucleic Acids Res, 43(7) (2015) e47.

[26] R. Kolde, pheatmap: Pretty Heatmaps, (2019). https://CRAN.R-project.org/package=pheatmap.

[27] E.K. Gustavsson, D. Zhang, R.H. Reynolds, S. Garcia-Ruiz, M. Ryten, ggtranscript: an R package for the visualization and interpretation of transcript isoforms using ggplot2, Bioinformatics, 38(15) (2022) 3844-3846.

[28] P. Langfelder, S. Horvath, WGCNA: an R package for weighted correlation network analysis, BMC Bioinformatics, 9 (2008) 559.

[29] D. He, Q. Li, G. Du, G. Meng, J. Sun, S. Chen, An Integration of Network Pharmacology and Experimental Verification to Investigate the Mechanism of Guizhi to Treat Nephrotic Syndrome, Front Pharmacol, 12 (2021) 755421.

[30] G. Yu, L.G. Wang, Y. Han, Q.Y. He, clusterProfiler: an R package for comparing biological themes among gene clusters, Omics, 16(5) (2012) 284-7.

[31] M. Zhu, Q. Zeng, T. Fan, Y. Lei, F. Wang, S. Zheng, X. Wang, H. Zeng, F. Tan, N. Sun, Q. Xue, J. He, Clinical Significance and Immunometabolism Landscapes of a Novel Recurrence-Associated Lipid Metabolism Signature In Early-Stage Lung Adenocarcinoma: A Comprehensive Analysis, Front Immunol, 13 (2022) 783495.

[32] N.T. Doncheva, J.H. Morris, J. Gorodkin, L.J. Jensen, Cytoscape StringApp: Network Analysis and Visualization of Proteomics Data, J Proteome Res, 18(2) (2019) 623-632.

[33] J. Friedman, T. Hastie, R. Tibshirani, Regularization Paths for Generalized Linear Models via Coordinate Descent, J Stat Softw, 33(1) (2010) 1-22.

[34] M.B. Kursa, Robustness of Random Forest-based gene selection methods, BMC Bioinformatics, 15 (2014) 8.

[35] M.L. Huang, Y.H. Hung, W.M. Lee, R.K. Li, B.R. Jiang, SVM-RFE based feature selection and Taguchi parameters optimization for multiclass SVM classifier, ScientificWorldJournal, 2014 (2014) 795624.

[36] M.a.W. Kuhn, Hadley, parsnip: A tidy unified interface to models, (2020). https://CRAN.R-project.org/package=parsnip.

[37] M. Yoo, J. Shin, J. Kim, K.A. Ryall, K. Lee, S. Lee, M. Jeon, J. Kang, A.C. Tan, DSigDB: drug signatures database for gene set analysis, Bioinformatics, 31(18) (2015) 3069-71.

[38] E.Y. Chen, C.M. Tan, Y. Kou, Q. Duan, Z. Wang, G.V. Meirelles, N.R. Clark, A. Ma'ayan, Enrichr: interactive and collaborative HTML5 gene list enrichment analysis tool, BMC Bioinformatics, 14 (2013) 128.

[39] T. Su, Y. He, M. Wang, H. Zhou, Y. Huang, M. Ye, Q. Guo, Y. Xiao, G. Cai, M. Zhao, J. Wang, X. Luo, Macrophage-Hepatocyte Circuits Mediated by Grancalcin Aggravate the Progression of Metabolic Dysfunction Associated Steatohepatitis, Adv Sci (Weinh), 11(42) (2024) e2406500.

[40] R.L. Philips, Y. Wang, H. Cheon, Y. Kanno, M. Gadina, V. Sartorelli, C.M. Horvath, J.E. Darnell, Jr., G.R. Stark, J.J. O'Shea, The JAK-STAT pathway at 30: Much learned, much more to do, Cell, 185(21) (2022) 3857-3876.

ISSN 2618-1584 Vol. 7, Issue 6: 1-14, DOI: 10.25236/FMSR.2025.070601

[41] D. Liu, P. Zhang, J. Zhou, R. Liao, Y. Che, M.M. Gao, J. Sun, J. Cai, X. Cheng, Y. Huang, G. Chen, H. Nie, Y.X. Ji, X.J. Zhang, Z. Huang, H. Xu, Z.G. She, H. Li, TNFAIP3 Interacting Protein 3 Overexpression Suppresses Nonalcoholic Steatohepatitis by Blocking TAK1 Activation, Cell Metab, 31(4) (2020) 726-740.e8.

[42] L. Vande Walle, N. Van Opdenbosch, P. Jacques, A. Fossoul, E. Verheugen, P. Vogel, R. Beyaert, D. Elewaut, T.D. Kanneganti, G. van Loo, M. Lamkanfi, Negative regulation of the NLRP3 inflammasome by A20 protects against arthritis, Nature, 512(7512) (2014) 69-73.

[43] N. Sharma, R. Sistla, S.B. Andugulapati, Yohimbine ameliorates liver inflammation and fibrosis by regulating oxidative stress and Wnt/β-catenin pathway, Phytomedicine, 123 (2024) 155182.

[44] T. Liu, L. Zhang, D. Joo, S.C. Sun, NF-κB signaling in inflammation, Signal Transduct Target Ther, 2 (2017) 17023.

[45] G. Yuan, Q. Qiao, A. Jiang, Z. Jiang, H. Luo, L. Huang, J. Wang, Y. Jiang, LPS-induced extracellular AREG triggers macrophage pyroptosis through the EGFR/TLR4 signaling pathway, Front Immunol, 16 (2025) 1549749.

[46] X. Wu, Z.H. Yang, J. Wu, J. Han, Ribosome-rescuer PELO catalyzes the oligomeric assembly of NOD-like receptor family proteins via activating their ATPase enzymatic activity, Immunity, 56(5) (2023) 926-943.e7.

[47] M. Xu, R. Gong, J. Xie, S. Xu, S. Wang, Clinical characteristics of lean and non-lean non-alcoholic fatty liver disease: a cross-sectional study, Nutr Metab (Lond), 22(1) (2025) 40.

[48] R. Zhang, R. Kang, D. Tang, Gut Microbiome Mediates Ferroptosis Resistance for Colorectal Cancer Development, Cancer Res, 84(6) (2024) 796-797.

[49] B. Wang, Z.H. Liu, J.J. Li, J.X. Xu, Y.M. Guo, J.X. Zhang, T. Chu, Z.F. Feng, Q.Y. Jiang, D.D. Wu, Role of ferroptosis in breast cancer: Molecular mechanisms and therapeutic interventions, Cell Signal, 134 (2025) 111869.

[50] Y. Hong, Q. An, Z. Wang, B. Hu, Y. Yang, R. Zeng, Y. Yao, Multi-omics Analysis Reveals the Propagation Mechanism of Ferroptosis in Acute Kidney Injury, Inflammation, (2025).

[51] F. Zhang, E.K.K. Lo, C. Chen, J.C. Lee, Felicianna, M.J. Ismaiah, H.K.M. Leung, D.H.L. Tsang, H. El-Nezami, Probiotics Mixture, Prohep: a Potential Adjuvant for Low-Dose Sorafenib in Metabolic Dysfunction-Associated Steatotic Liver Disease-Associated Hepatocellular Carcinoma Suppression Through Modulating Gut Microbiota, Probiotics Antimicrob Proteins, (2025).

[52] S.J. Dixon, K.M. Lemberg, M.R. Lamprecht, R. Skouta, E.M. Zaitsev, C.E. Gleason, D.N. Patel, A.J. Bauer, A.M. Cantley, W.S. Yang, B. Morrison, 3rd, B.R. Stockwell, Ferroptosis: an iron-dependent form of nonapoptotic cell death, Cell, 149(5) (2012) 1060-72.

[53] J.P. Iredale, Models of liver fibrosis: exploring the dynamic nature of inflammation and repair in a solid organ, J Clin Invest, 117(3) (2007) 539-48.

[54] Y. Du, Z. Guo, Recent progress in ferroptosis: inducers and inhibitors, Cell Death Discov, 8(1) (2022) 501.

[55] Y. Xu, J. Chen, W. Jiang, Y. Zhao, C. Yang, Y. Wu, Q. Li, C. Zhu, Multiplexing Nanodrug Ameliorates Liver Fibrosis via ROS Elimination and Inflammation Suppression, Small, 18(3) (2022) e2102848.

[56] W. Tang, Z. Zhao, Y. Chong, C. Wu, Q. Liu, J. Yang, R. Zhou, Z.X. Lian, G. Liang, Tandem Enzymatic Self-Assembly and Slow Release of Dexamethasone Enhances Its Antihepatic Fibrosis Effect, ACS Nano, 12(10) (2018) 9966-9973.